

A Hierarchical Coding Scheme for Glasses-free 3D Displays Based on Scalable Hybrid Layered Representation of Real-World Light Fields

Joshitha R* and Mansi Sharma*

Abstract—This paper presents a novel hierarchical coding scheme for light fields based on transmittance patterns of low-rank multiplicative layers and Fourier disparity layers. The proposed scheme learns stacked multiplicative layers from subsets of light field views determined from different scanning orders. The multiplicative layers are optimized using a fast data-driven convolutional neural network (CNN). The essential factor for multiplicative layers representation, which has not been considered in previous compression approaches, is the origin of redundancy, *i.e.*, the low rank structure of light field data. The spatial correlation in layer patterns is exploited with varying low ranks in factorization derived from singular value decomposition on a Krylov subspace. Further, encoding with HEVC efficiently removes intra-view and inter-view correlation in low-rank approximated layers. The initial subset of approximated decoded views from multiplicative representation is used to construct Fourier disparity layer (FDL) representation. The FDL model synthesizes second subset of views which is identified by a pre-defined hierarchical prediction order. The correlations between the prediction residue of synthesized views is further eliminated by encoding the residual signal. The set of views obtained from decoding the residual is employed in order to refine the FDL model and predict the next subset of views with improved accuracy. This hierarchical procedure is repeated until all light field views are encoded. The critical advantage of proposed hybrid layered representation and coding scheme is that it utilizes not just spatial and temporal redundancies, but efficiently exploits the strong intrinsic similarities among neighboring sub-aperture images in both horizontal and vertical directions as specified by different predication orders. Besides, the scheme is flexible to realize a range of multiple bitrates at the decoder within a single integrated system. The compression performance analyzed with real light field shows substantial bitrate savings, maintaining good reconstruction quality.

I. INTRODUCTION

The market of glasses-free displays is growing rapidly in recent years. Current generation autostereoscopic display techniques are seen as an alternative to stereoscopic 3D as it supports both stereopsis and motion parallax with many views for different viewing directions. However, technology has still not matured enough to simultaneously provide direction-dependent outputs without sacrificing the resolution in reconstructing the dense light fields. Emerging multi-layered light field displays offer solution that provides continuous motion parallax, greater depth-of-field, and wider field-of-view [1]–[3]. A typical structure of a multi-layered display is shown in Fig. 1a. It consists of light-attenuating

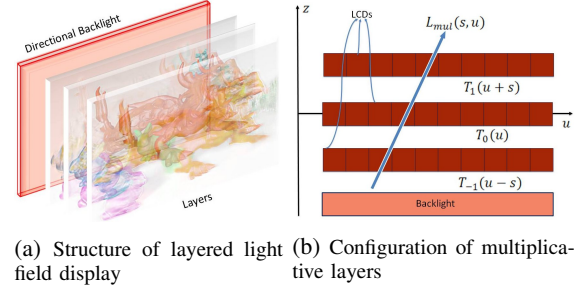


Fig. 1: Multiplicative layer patterns for layered light field display.

layers stacked in front of a backlight. On each layer, the transmittance of pixels can be controlled independently by carrying out multiplicative operations on the layered patterns. Fig. 1b illustrates the light rays which pass through different combinations of pixels in stacked layers depending on the viewing directions. Layered displays accurately reproduce multi-view images or light field simultaneously with high resolution using just few light attenuating layers. Efficient representation and coding of light rays in multi-layered 3D displays is critical for its adaptation on different autostereoscopic platforms.

Existing light field coding algorithms are broadly categorized into approaches using the lenslet image [4]–[6] or sub-aperture images (SAIs). We can further classify compression methods exploiting geometry information [7]–[11], scene content information [12], view prediction based learning schemes [13]–[16] or methods considering light field data as a pseudo video sequence [17]–[20]. The approaches arranging SAIs as pseudo-temporal sequence are constrained to one-dimensional coding structure. Nonlinear correlation in horizontal and vertical directions among adjacent SAIs are not carefully considered in their coding models. The geometry-based or learning-based methods usually demand accurate mathematical model for parameter estimation or suffer from the primary limitation of low quality reconstruction. Their suitability is questionable for compactly encoding light fields with multiple bitrates dealing with layered structure of transmittance patterns in multi-layered displays.

In this paper, we propose a novel hierarchical coding scheme for light fields based on multiplicative layers [21] and Fourier disparity layers representation [22]. The input light field is divided into two subsets based on predefined Circular and Hierarchical prediction orders (Fig. 4). A data-driven convolutional neural network (CNN) is optimized to learn three multiplicative layers for each view subset. The key idea

* The authors contributed equally to the work.

Joshitha R and Mansi Sharma are with the Department of Electrical Engineering, Indian Institute of Technology Madras, Chennai 600036, India. (email: ee19d401@smail.iitm.ac.in, mansisharmaitd@gmail.com)

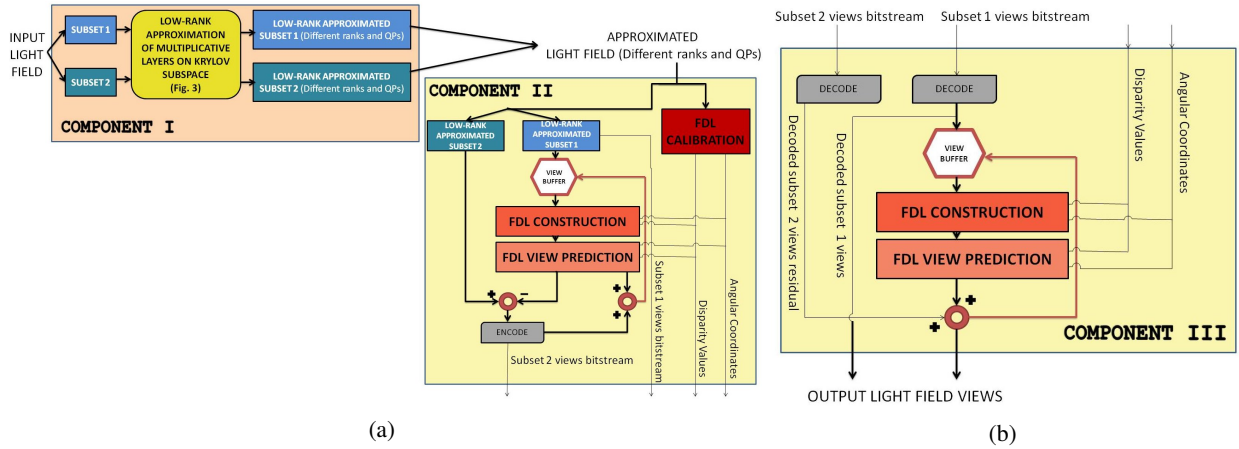


Fig. 2: The three components of the overall workflow of proposed coding scheme. (a) Overview of the encoding scheme. The low rank approximation of multiplicative layers on Krylov subspace (block in chrome yellow) is expanded in Fig. 3 (b) Overview of the decoding scheme.

is to reduce dimensionality of stacked multiplicative layers using a randomized block Krylov singular value decomposition (BK-SVD) procedure [23]. Factorization derived from the BK-SVD efficiently exploits the high spatial correlation between multiplicative layers on Krylov subspaces and approximate light fields for varying low ranks. Encoding of these approximated layers using HEVC codec [24] further eliminates intra-view and inter-view redundancies. In the first stage, the proposed scheme approximates multiplicative layers of a target light field for multiple ranks and the quantization parameters (QPs). The view subsets are reconstructed from the decoded layers.

In the second stage, the entire approximated light field is processed in the Fourier domain following a hierarchical coding procedure. A Fourier Disparity Layer (FDL) calibration estimates disparity values and angular coordinates of each light field view [25]. These parameters provide additional information for FDL construction and view prediction. These parameters are transmitted to the decoder as metadata. We then split the approximated light field into subsets as identified with scanning and prediction orders. The first set of views is encoded and used for construction of the FDL representation. This FDL representation is used to synthesize the second subset. The remaining correlations between the prediction residue of synthesized views is further eliminated by encoding the residual signal using HEVC with inter coding mode. The set of views obtained from decoding the residual are employed in order to refine the FDL representation and predict the next subset of views with improved accuracy. This hierarchical procedure continues iterating until all light field views are coded. The critical advantages of the proposed hybrid layered representation and coding scheme are:

- It efficiently exploits the strong intrinsic similarities in light field structure by approximating multiplicative layer patterns with varying low ranks. Moreover, it ensures inter-view prediction from adjacent views (both horizontally and vertically) that exhibit higher

similarity. The results with different scanning orders demonstrates high compression performance on real world light field data.

- It is flexible to realize a range of multiple bitrates within a single integrated system trained using few (two) convolutional neural networks. This critical characteristic of the proposed model complements existing light field coding systems or methods which support only specific bitrates during the compression. This would offer an adaptation of layered displays to support a variety of computational or multi-view auto-stereoscopic platforms by optimizing the bandwidth for a given target bitrate.

II. PROPOSED SCHEME

The overall workflow of our proposed representation and coding scheme is illustrated in Fig. 2. The scheme is divided into three primary components. In **COMPONENT I**, input light field images are divided into subsets, specified by different view prediction orders. The **COMPONENT I** is further expanded into three blocks as depicted in Fig. 3. This component performs low-rank approximation of different subsets of the input light field. The **BLOCK I** represents a CNN that converts the light field views of the input subsets into three multiplicative layers [21]. In **BLOCK II**, the intrinsic redundancy present in subset views is removed by exploiting the hidden low-rank structure of multiplicative layers on a Krylov subspace for various ranks [23]. HEVC [24] encoding of low-rank approximated multiplicative layers further eliminates the inter-frame and intra-frame redundancies in low-rank approximated layers. In **BLOCK III**, the approximated views of the subset are reconstructed from the decoded layers. The entire approximated light field is obtained at the end of **COMPONENT I**.

The approximated subset of decoded views obtained from **COMPONENT I** following multiplicative layer representation is used to construct Fourier disparity layer (FDL) [22] representation in **COMPONENT II**. The processing of approximated light field in **COMPONENT II** of our scheme

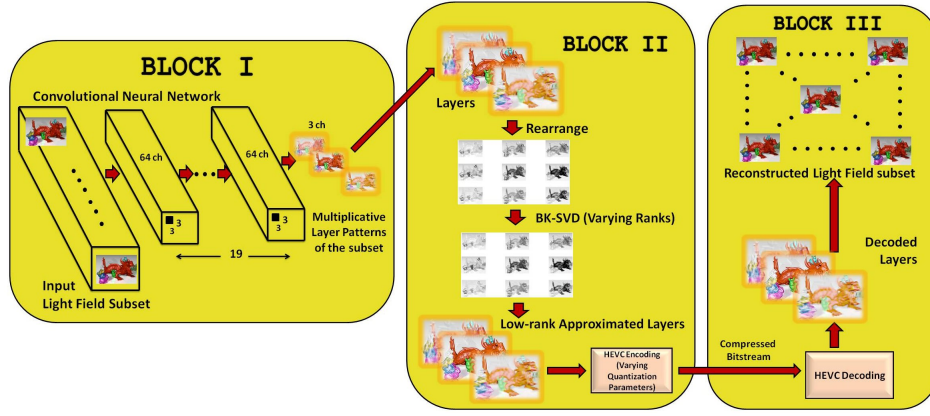


Fig. 3: The low rank approximation of multiplicative layers on Krylov subspace consists of three blocks: conversion of light field views into multiplicative layers, low-rank approximation of layers & HEVC encoding, and the decoding of the approximated layers followed by the reconstruction of the light field.

is shown in Fig. 2a. There exist strong intrinsic similarities between neighboring sub-aperture images in both horizontal and vertical directions as specified by different predication orders. The main functionality of *COMPONENT II* is to further eliminate inter-view redundancy from low-rank approximated adjacent views as possible determined from different scanning orders. Following a hierarchical procedure, the FDL representation reconstructs the light field iteratively.

The angular coordinates and disparity values of each view of the low-rank approximated light field (at different ranks and QPs) are determined through FDL calibration and directly transmitted to the decoder (*COMPONENT III*) as metadata [25]. The approximated light field is divided into two subsets specified by prediction order. Subset 1 aids in constructing the FDL representation, which is further used to synthesize the second subset of views. The encoding of the residual signal is performed to account for the correlations in the prediction residue of synthesized Subset 2. A more accurate FDL representation is built from previously encoded subsets. Thus, there is an iterative refinement of the FDL representation in *COMPONENT II* until all the approximated light field views are encoded. Our decoding scheme is depicted in the *COMPONENT III* (Fig. 2b). The angular coordinates and disparity values of the low-rank approximated light field, along with the encoded bitstreams of approximated Subset 1 and Subset 2, are utilized for the final reconstruction.

A. Approximation of light field at different ranks

COMPONENT I illustrates the division of input light field into two subsets and their low-rank approximation in the Block-Krylov subspace. As shown in Fig. 3, this step involves three blocks that are described in the following sub-sections.

1) *View Subsets of Light Field:* Dib et al. [25] recommend two best scanning orders for synthesizing and coding view subsets, Circular-2 (C_2) and Hierarchical-2 (H_2). For a 9×9 light field, the C_2 pattern contains two subsets. The first subset forms a circular pattern, and the remaining views constitute the second subset. The H_2 configuration follows a

more simple division of subsets, where each subset comprises of alternate views. The exact coding orders of each subset of the C_2 and H_2 patterns are shown in Fig. 4. In both patterns, the views are ordered beginning with the central view and spiraling out towards the periphery for each subset. Our proposed workflow (Fig. 2) begins with partitioning of the input light field into two subsets based on the C_2 or H_2 pattern, which are then approximated by BK-SVD.

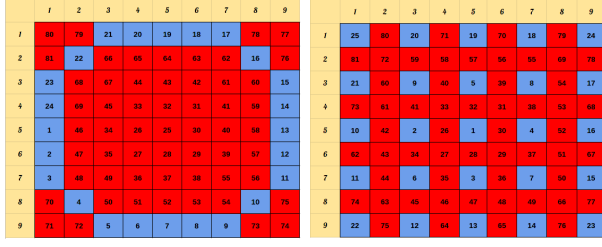
2) *Light Field Views to Stacked Multiplicative Layers:* The four-dimensional light field $L(u, v, s, t)$ is parameterized by angular coordinates (u, v) and spatial coordinates (s, t) [26], [27]. If the (s, t) plane is located at depth z , the light ray will have coordinates $(u + zs, v + zt)$ (Fig. 5).

Multiplicative layers [21] are light attenuating panels that are stacked in evenly spaced intervals in front of a backlight as shown in Fig. 1. The transmittance of a multiplicative layer M_z is given by $M_z(u, v)$ and a light ray emitted from these layers will have intensity

$$L_{mul}(u, v, s, t) = \prod_{z \in Z} M_z(u + zs, v + zt) \quad (1)$$

where, z is the disparity among directional views and Z denotes a set of z . In our work, we considered the two subsets of the light field as $L_1(u, v, s, t)$ and $L_2(u, v, s, t)$. Three multiplicative layers located at $Z = \{-1, 0, 1\}$ for each of the two input subsets are obtained. These multiplicative layer patterns are enough to efficiently represent each subset entirely. We performed the optimization of the three layer patterns for each light field by training two CNNs. The final trained network can convert each of the light field subsets into three optimized output multiplicative layers as depicted in *BLOCK I* of Fig. 3.

3) *Low Rank Representation and Coding of Stacked Multiplicative Layers on Krylov Subspace:* The key idea of the proposed scheme is to remove the intrinsic redundancy in light field multiplicative layers by compactly representing them on a Krylov subspace. The randomised Block-Krylov SVD introduced by Cameron Musco and Christopher Musco [23] can optimally achieve the low-rank approximation of a matrix within $(1 + \epsilon)$ of optimal for spectral norm



(a) Circular-2

(b) Hierarchical-2

Fig. 4: View subsets for the two chosen prediction orders, Circular-2 and Hierarchical-2. Views in blue form the first subset and views in red form the second subset.

error. The algorithm quickly converges in $\tilde{O}(\frac{1}{\sqrt{\epsilon}})$ iterations for any matrix.

In our proposed scheme, we denote each multiplicative layer pattern produced by the CNN as $M_z \in \mathbb{R}^{m \times n \times 3}$, where $z \in \{-1, 0, 1\}$. The red, green, and blue colour channels of the layer z are denoted as M_z^r , M_z^g , and M_z^b respectively. We constructed three matrices $B^{ch} \in \mathbb{R}^{3m \times n}$, $ch \in \{r, g, b\}$, as

$$B^{ch} = \begin{pmatrix} M_1^{ch} \\ M_0^{ch} \\ M_{-1}^{ch} \end{pmatrix} \quad (2)$$

The intrinsic redundancies in multiplicative layers of the light field can be effectively removed by following low-rank BK-SVD approximation in a Krylov subspace for each B^{ch} , $ch \in \{r, g, b\}$. For simplicity, we will denote B^{ch} as B henceforth. Our present formulation of low-rank light field layer approximation seeks to find a subspace that closely captures the variance of B 's top singular vectors and avoid the gap dependence in singular values. We target spectral norm low-rank approximation error of B , defined as

$$\|B - WW^T B\|_2 \leq (1 + \epsilon) \|B - B_k\|_2 \quad (3)$$

where, W is a rank k matrix with orthonormal columns. In a rank k approximation, only the top k singular vectors of B are considered relevant and the spectral norm guarantee ensures that $WW^T B$ recovers B up to a threshold ϵ . We start with a random matrix $\Pi \sim N(0, 1)^{d \times k}$ and perform Block Krylov Iteration by working with the Krylov subspace,

$$K = [\Pi \quad B_z \Pi \quad B_z^2 \Pi \quad B_z^3 \Pi \cdots B_z^q \Pi] \quad (4)$$

We constructed $p_q(B)\Pi$ for any polynomial $p_q(\cdot)$ of degree q by working with Krylov subspace K . The approximation of matrix B done by projecting it onto the span of $p_q(B)\Pi$, is similar to the best k rank approximation of B lying in the span of the Krylov space K . Thus, the nearly optimal low-rank approximation of B can be achieved by finding this best rank k approximation. To ensure that the best spectral norm error low-rank approximation lies in the span of K , we orthonormalized the columns of K to obtain $Q \in \mathbb{R}^{c \times qk}$ using the QR decomposition method [28]. We take SVD of matrix $S = Q^T B B^T Q$ where, $S \in \mathbb{R}^{qk \times qk}$, for faster computation and accuracy. The rank k approximation

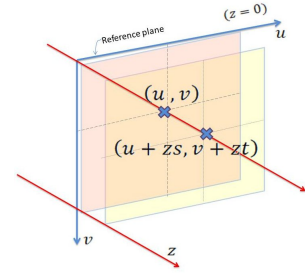


Fig. 5: The light ray is parameterized by point of intersection with the (u, v) plane and the (s, t) plane located at a depth z .

of B is matrix W , which is obtained as

$$W = Q \bar{U}_k \quad (5)$$

where, \bar{U}_k is set to be the top k singular vectors of S . Consequently, the rank k block Krylov approximation of matrices B^r , B^g and B^b are W^r , W^g , and W^b respectively. The $W^{ch} \in \mathbb{R}^{x \times y}$ for every colour channel ch .

To obtain the approximated layers \hat{M}_z , $z \in \{-1, 0, 1\}$, we extract their colour channels from the approximated W^{ch} matrices by sectioning out the rows uniformly as

$$\hat{M}_{-1}^{ch} = W^{ch}[1 : x, 1 : y] \quad (6a)$$

$$\hat{M}_0^{ch} = W^{ch}[x + 1 : 2x, 1 : y] \quad (6b)$$

$$\hat{M}_1^{ch} = W^{ch}[2x + 1 : 3x, 1 : y] \quad (6c)$$

The red, green, and blue colour channels are then combined to form each approximated layer \hat{M}_{-1} , \hat{M}_0 , and \hat{M}_1 . Thus, factorization derived from the BK-SVD exploits the spatial correlation in multiplicative layers of the subset views for varying low ranks. The three block Krylov approximated layers for each subset are subsequently encoded into a bitstream using HEVC [24] for various QPs to further eliminate inter and intra layer redundancies in the low-rank approximated representation. We have shown this low-rank representation and coding of stacked multiplicative layers on Krylov subspace in *BLOCK II* of Fig. 3.

4) Decoding and Reconstruction of the Light Field Subsets: The decoding procedure of compressed layers and the reconstruction of light field subset is illustrated in *BLOCK III* of Fig. 3. We decoded three layers from the bitstream and converted them into the RGB format. The decoded layers are denoted as \hat{M}_z , where $z \in \{-1, 0, 1\}$ depicts the depth of the layers. To reconstruct the views of each subset, we considered the integers s^*, t^* (which depend on the number of views in the subset). The view $I_{(s^*, t^*)}$ is obtained by translating the decoded layers to \hat{M}_z and performing an element-wise product of the colour channels of the translated layers. For a particular view (s^*, t^*) , the translation of every z^{th} layer \hat{M}_z , to \bar{M}_z is carried out as

$$\bar{M}_{z(s^*, t^*)}(u, v) = \hat{M}_z(u + zs^*, v + zt^*) \quad (7)$$

Thus, the three translated layers for every viewpoint (s^*, t^*) are

$$\begin{aligned}\bar{M}_{-1(s^*, t^*)}(u, v) &= \dot{M}_{-1}(u - s^*, v - t^*) \\ \bar{M}_{0(s^*, t^*)}(u, v) &= \dot{M}_0(u, v) \\ \bar{M}_{1(s^*, t^*)}(u, v) &= \dot{M}_1(u + s^*, v + t^*)\end{aligned}$$

An element-wise product of each colour channel $ch \in \{r, g, b\}$, of the translated layers gives the corresponding colour channel of the subset view.

$$I_{(s^*, t^*)}^{ch} = \bar{M}_{-1(s^*, t^*)}^{ch} \odot \bar{M}_{0(s^*, t^*)}^{ch} \odot \bar{M}_{1(s^*, t^*)}^{ch} \quad (8)$$

The combined red, green, and blue colour channels output the reconstructed light field subset at the viewpoint (s^*, t^*) as $I_{(s^*, t^*)}$. Subsets 1 and 2 are then merged according to the Circular-2 (C_2) or Hierarchical-2 (H_2) ordering.

COMPONENT I of the proposed scheme, hence, exploits the spatial correlation in multiplicative layers of the subset views for varying low ranks. Inter and intra layer redundancies in the low-rank approximated representation are removed as well. We further compress the light field by eliminating intrinsic similarities among neighboring views of the C_2 or H_2 patterns (in both horizontal and vertical directions) using the Fourier Disparity Layers representation.

B. Fourier Disparity Layers (FDL) Representation

The Fourier Disparity Layers representation [22] samples the input BK-SVD approximated light field in the disparity dimension by decomposing it as a discrete sum of layers. The decomposition is carried out in the Fourier domain and FDL representation is constructed by a regularized least square regression performed independently at each spatial frequency. *COMPONENT II* in Fig. 2a summarises the use of FDL and encoding of low-rank approximated subsets. We highlight the FDL calibration, subset view synthesis and prediction in the following subsections.

1) *FDL Calibration*: Construction of the FDL requires the angular coordinates u_j of the input approximated light field views and the disparity values d_k of the layers. These parameters are found by minimizing over all frequency components f_s of each view [25]. The view L_{u_o} of the approximated light field at angular coordinate u_o can be defined as $L_{u_o}(s) = L(s, u_o)$ and by using n disparity values $\{d_k\}_{k \in [1, n]}$, the Fourier transform of L_{u_o} can be written as

$$\hat{L}_{u_o}(f_s) = \sum_k e^{+2i\pi u_o d_k f_s} \hat{L}^k(f_s) \quad (9)$$

where, f_s is the spatial domain frequency. The Fourier transform of the central light field view obtained by only considering a specific spatial region of disparity d_k is given by each \hat{L}^k .

By computing the Fourier transforms of all m approximated light field views as $\hat{L}_{u_j}(j \in [1, m])$, the FDL representation can be learnt by solving a linear regression problem for each frequency f_s . The problem is formulated by $\mathbf{Ax} = \mathbf{b}$ with Tikhonov regularization where $\mathbf{A} \in \mathbb{R}^{m \times n}$, $\mathbf{x} \in \mathbb{R}^{n \times 1}$ and $\mathbf{b} \in \mathbb{R}^{m \times 1}$. Elements of matrix \mathbf{A} are

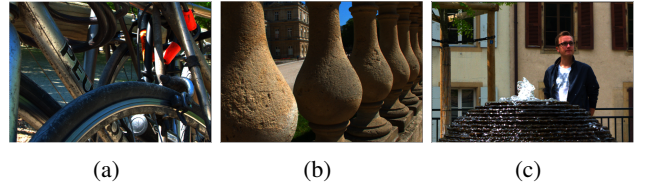


Fig. 6: Central views of the three datasets (a) Bikes, (b) Stone pillars outside, (c) Fountain & Vincent 2.

$\mathbf{A}_{jk} = e^{+2i\pi u_j d_k f_s}$, \mathbf{x} contains the Fourier coefficients of disparity layers $\mathbf{x}_k = \hat{L}^k(f_s)$ and Fourier coefficients of the j^{th} input view, $\mathbf{b}_j = \hat{L}_{u_j}(f_s)$ are contained in \mathbf{b} .

2) *FDL View Synthesis and Prediction*: Any subset view L_{u_o} at angular coordinate u_o can be synthesized in the Fourier domain with the FDL and their disparities d_k using Eq. 9. The C_2 and H_2 prediction orders divide the low-rank approximated light field into two subsets. The first approximated subset is encoded and aids in constructing the FDL representation. The second approximated subset views are then synthesized using the FDL and the residual signal further refines the representation through iterative encoding of each view. We send the bitstreams of each approximated subsets along with the encoded metadata of parameters to the decoding end, *COMPONENT III* of Fig. 2b.

III. RESULTS AND ANALYSIS

The performance of the proposed compression scheme was evaluated on real light fields captured by plenoptic cameras. We experimented with *Bikes*, *Fountain & Vincent 2*, and *Stone pillars outside* light field datasets from the EPFL Lightfield JPEG Pleno database [29]. Fig. 6 shows the central views of the chosen light field images. The raw plenoptic images were extracted into 15×15 sub-aperture views using the Matlab Light field toolbox [30]. The C_2 and H_2 coding patterns were constructed from the inner 9×9 views for our tests.

A. Experimental Settings and Implementation Details

The proposed scheme was implemented on a single high-end HP OMEN X 15-DG0018TX system with 9th Gen i7-9750H, 16 GB RAM, RTX 2080 8 GB Graphics, and Windows 10 operating system. We optimized the multiplicative layer patterns for each subset using CNN with twenty 2-D convolutional layers stacked in a sequence. The CNN models were trained for 25 epochs at a learning rate of 0.001 and a batch size of 15. The entire network was implemented using the Python-based framework, Chainer (version 7.7.0).

The resultant output multiplicative layers for each subset of the C_2 and H_2 patterns were obtained from the trained CNN models. We rearranged the colour channels of these multiplicative layers as described in section II-A.3 and then applied BK-SVD for ranks 4, 8, 16, 28, 44, 52 and 60. The approximated matrices were then arranged back into layers and compressed using HEVC HM 11.0 (*BLOCK II* of *COMPONENT I*). We used quantization parameters 2, 6, 10, 14, 20, 26, and 38 to test both high and low bitrate

TABLE I: The total number of bytes written to file for each subset of the Circular-2 pattern using our proposed coding scheme and Dib et al. [25].

QP	Scheme	Bikes		Stone pillars outside		Fountain & Vincent 2	
		Subset 1	Subset 2	Subset 1	Subset 2	Subset 1	Subset 2
2	Dib et al.	6373276	9269248	6321523	7928095	6912472	8363327
	Proposed (Rank 4)	1634865	285016	1358448	243122	1827059	335430
	Proposed (Rank 8)	1877550	349216	1512085	283331	2115774	380847
	Proposed (Rank 16)	2177689	417666	1847285	351680	2519102	446949
	Proposed (Rank 28)	2438540	486569	2142502	418877	2806767	494263
	Proposed (Rank 44)	2674089	532163	2350849	487484	3008060	545947
	Proposed (Rank 52)	2749844	561758	2401859	503039	3063768	535674
6	Dib et al.	2805401	581882	2448047	527789	3113991	535619
	Proposed (Rank 4)	4350810	5663692	4354754	4732850	4869817	4963030
	Proposed (Rank 8)	602334	124074	493765	104272	728339	149454
	Proposed (Rank 16)	741293	165605	571942	130267	893240	178163
	Proposed (Rank 28)	916846	211107	761895	173837	1138839	220365
	Proposed (Rank 44)	1086119	247005	925727	218830	1349095	252514
	Proposed (Rank 52)	1252891	282873	1051703	256343	1499318	268165
10	Dib et al.	1311143	290011	1084796	268153	1547468	279455
	Proposed (Rank 4)	1354933	310371	1118995	281491	1583718	284981
	Proposed (Rank 8)	4350810	5663692	4354754	4732850	4869817	4963030
	Proposed (Rank 16)	602334	124074	493765	104272	728339	149454
	Proposed (Rank 28)	741293	165605	571942	130267	893240	178163
	Proposed (Rank 44)	916846	211107	761895	173837	1138839	220365
	Proposed (Rank 52)	1086119	247005	925727	218830	1349095	252514
14	Dib et al.	1252891	282873	1051703	256343	1499318	268165
	Proposed (Rank 4)	1311143	290011	1084796	268153	1547468	279455
	Proposed (Rank 8)	1354933	310371	1118995	281491	1583718	284981
	Proposed (Rank 16)	1635624	1555027	1697516	1227782	1879832	1231959
	Proposed (Rank 28)	85418	47842	60119	36583	124338	51127
	Proposed (Rank 44)	129326	64433	81540	45979	177036	66168
	Proposed (Rank 52)	197901	80959	136933	64691	279887	79125
20	Dib et al.	271565	98486	200957	79562	376807	94429
	Proposed (Rank 4)	347606	112747	255491	93448	449040	103222
	Proposed (Rank 8)	372263	119795	267999	97639	466826	103998
	Proposed (Rank 16)	389902	127835	280325	102454	483184	107398
	Proposed (Rank 28)	1635624	1555027	1697516	1227782	1879832	1231959
	Proposed (Rank 44)	85418	47842	25871	19602	54329	33592
	Proposed (Rank 52)	129326	64433	34316	23444	76408	33557
26	Dib et al.	197901	80959	55115	31584	116924	40566
	Proposed (Rank 4)	271565	98486	77665	38192	160911	47636
	Proposed (Rank 8)	347606	112747	99503	44221	187776	51037
	Proposed (Rank 16)	372263	119795	104642	46549	195728	52069
	Proposed (Rank 28)	389902	127835	109416	48116	203384	51973
	Proposed (Rank 44)	191049	125748	180485	56164	213553	66399
	Proposed (Rank 52)	18109	15295	12194	10550	26763	14884
38	Dib et al.	26471	20342	16372	13010	35126	18824
	Proposed (Rank 4)	36035	24566	22220	15325	46554	19651
	Proposed (Rank 8)	46328	28090	28818	17922	60959	23291
	Proposed (Rank 16)	55291	29746	35061	20507	70030	24332
	Proposed (Rank 28)	58525	30369	37056	20533	73670	24606
	Proposed (Rank 44)	61024	33935	39291	21200	75358	25193
	Proposed (Rank 52)	23065	7880	12613	1880	22582	2155

cases of HEVC. The decoding and reconstruction of BK-SVD approximated subsets for both C_2 and H_2 patterns was performed.

Low-rank approximated subsets were then utilized to form the FDL representation of the light fields. The number of layers in the FDL method was fixed to $n = 30$. Views in approximated Subset 1 construct the initial FDL representation. Views of approximated Subset 2 are predicted from this FDL representation and the residues iteratively refine the FDL. We used HEVC HM 16.0 to perform the encoding in *COMPONENT II*, for quantization parameters 2, 6, 10, 14, 20, 26 and 38.

B. Results and Comparative Analysis

We compared the proposed scheme with the direct compression of light fields using FDL by Dib et al. [25]. The proposed coding scheme outperforms the anchor by large margins. The total number of bytes taken by our approach is comparatively far lesser than the work by Dib et al. [25] for all ranks and QPs. These corresponding results are highlighted in Table I for the (C_2) pattern and in Table II for (H_2) pattern. The bitrate vs YUV-PSNR graphs of the three datasets are illustrated in Fig. 7. For both the Circular-

TABLE II: Total number of bytes for each subset of Hierarchical-2 pattern using our proposed coding scheme and Dib et al. [25].

QP	Scheme	Bikes		Stone pillars outside		Fountain & Vincent 2	
		Subset 1	Subset 2	Subset 1	Subset 2	Subset 1	Subset 2
2	Dib et al.	8149470	9362963	8187441	7746889	8467600	8311549
	Proposed (Rank 4)	1752364	327571	1544489	277441	2000768	399280
	Proposed (Rank 8)	1923491	425176	1668430	336414	2197190	475908
	Proposed (Rank 16)	2132305	534173	1904622	452160	2413070	576114
	Proposed (Rank 28)	2307124	626191	2137972	550384	2589097	663419
	Proposed (Rank 44)	2466765	728164	2348147	638116	2701529	709257
	Proposed (Rank 52)	2531862	732311	2415703	670368	2728626	732779
6	Dib et al.	2572006	759606	2470431	700779	2741756	740021
	Proposed (Rank 4)	5968201	5584732	5943824	4566311	6317422	4734277
	Proposed (Rank 8)	696307	141510	600337	110556	870560	169079
	Proposed (Rank 16)	796855	191515	665513	143058	991937	208585
	Proposed (Rank 28)	928516	259814	809014	209917	1119092	266975
	Proposed (Rank 44)	1044367	309978	953162	267569	1237456	314759
	Proposed (Rank 52)	1151050	364678	1079187	314645	1320242	341091
10	Dib et al.	1195073	376134	1122665	337719	1345621	355264
	Proposed (Rank 4)	1224508	388297	1153867	350318	1356529	359455
	Proposed (Rank 8)	3906437	2991907	3972408	2394424	4256777	2365804
	Proposed (Rank 16)	178206	74529	139283	54783	278393	83747
	Proposed (Rank 28)	234038	103767	176282	74433	350782	106751
	Proposed (Rank 44)	313521	143968	251942	112280	442029	138069
	Proposed (Rank 52)	389826	175682	336035	146248	523367	166752
14	Dib et al.	465603	213126	423251	172780	582988	184091
	Proposed (Rank 4)	493156	213184	449828	182623	600907	187558
	Proposed (Rank 8)	515966	221252	476680	191252	606755	192677
	Proposed (Rank 16)	2265550	1479998	2432694	1068158	2505792	1058776
	Proposed (Rank 28)	80756	43910	56613	32851	125237	48892
	Proposed (Rank 44)	108524	61888	74445	41825	162045	61496
	Proposed (Rank 52)	150025	85871	111220	63932	212590	78435
20	Dib et al.	191702	105961	151212	82963	264760	93719
	Proposed (Rank 4)	228876	121783	194620	96725	297942	104203
	Proposed (Rank 8)	243903	126699	209660	101918	309631	106855
	Proposed (Rank 16)	254844	129017	222970	106454	314274	109546
	Proposed (Rank 28)	842135	459805	946011	221956	926805	286174
	Proposed (Rank 44)	31602	20923	21663	15803	50142	23547
	Proposed (Rank 52)	43511	29373	28169	19788	63745	29074
26	Dib et al.	60423	40866	40732	28521	83392	35879
	Proposed (Rank 4)	76647	49200	53703	35594	103900	42129
	Proposed (Rank 8)	89653	56477	66649	41210	118608	45865
	Proposed (Rank 16)	94969	59779	71693	42630	121445	47138
	Proposed (Rank 28)	98186	61299	75923	44694	124309	47441
	Proposed (Rank 44)	242763	111266	213782	28940	272168	50062
	Proposed (Rank 52)	13705	11349	9646	7203	20645	11951
38	Dib et al.	20006	14619	12592	9004	27722	14167
	Proposed (Rank 4)	26014	19172	15947	12784	32178	15899
	Proposed (Rank 8)	30615	22252	19394	14768	39019	17819
	Proposed (Rank 16)	34692	25694	23190	16965	42684	19317
	Proposed (Rank 28)	36820	26082	25005	17802	44419	19885
	Proposed (Rank 44)	37464	26717	26359	18185	45207	19866
	Proposed (Rank 52)	26295	6202	13132	2001	22971	1975

2 and Hierarchical-2 patterns, the proposed scheme has significantly better rate-distortion results.

Further, we analysed bitrate reduction (BD-rate) of the proposed scheme with respect to Dib et al. [25] using the Bjontgaard metric [31]. The average percent difference in rate change was estimated over a range of QPs for the seven chosen ranks. A comparison of the percentage of bitrate savings of our proposed coding scheme with respect to the anchor method for the three chosen light field datasets is shown in Table III. For the (C_2) pattern, the proposed scheme achieves 94.53%, 96.39%, and 93.96% bitrate reduction compared to Dib et al. [25] for the light fields *Bikes*, *Stone pillars outside*, and *Fountain & Vincent 2* respectively. For the pattern H_2 , the proposed scheme achieves 97.23%, 97.54%, and 96.67% bitrate reduction compared to Dib et al. [25] for the light fields *Bikes*, *Stone pillars outside*, and *Fountain & Vincent 2* respectively.

IV. CONCLUSION

We have proposed a novel hierarchical coding scheme for light fields based on transmittance patterns of low-rank multiplicative layers and Fourier disparity layers. Typical pseudo sequence-based light field compression schemes [17]–[20] do

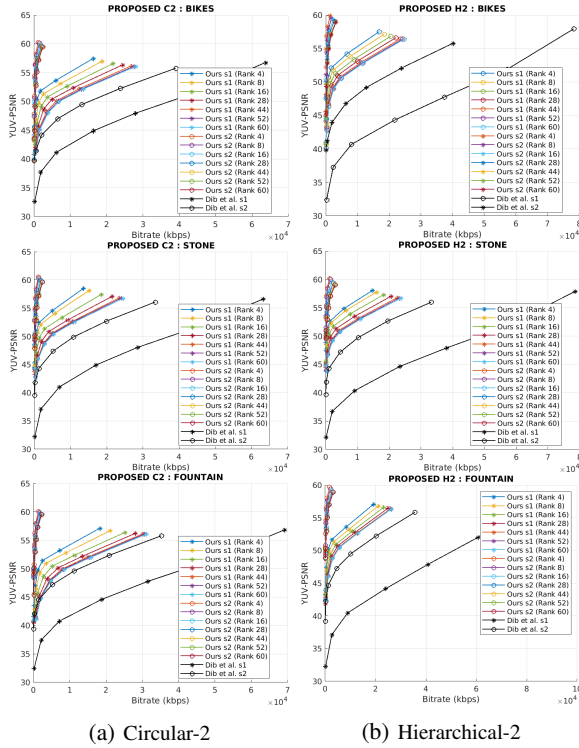


Fig. 7: Bitrate vs YUV-PSNR plots.

not efficiently consider the similarities between horizontal and vertical views of a light field. Our proposed scheme not only exploits the spatial correlation in multiplicative layers of the subset views for varying low ranks, but also removes the temporal inter and intra layer redundancies in the low-rank approximated representation of the view subsets. The approximated light field is further compressed by eliminating intrinsic similarities among neighboring views of the Circular-2 or Hierarchical-2 patterns using Fourier Disparity Layers representation. This integrated compression achieves excellent bitrate reductions without compromising the quality of the reconstructed light field.

Our scheme offers flexibility to cover a range of multiple bitrates using just two trained CNNs to obtain a layered representation of the light field subsets. This critical feature sets our proposed scheme apart from other existing light field coding methods, which usually train a system (or network) to support only specific bitrates during the compression. Besides, existing coding approaches are not explicitly designed to target layered displays and are usually only classified to work for lenslet-based formats or sub-aperture images based pseudo-sequence light field representation. Our coding model can complement existing layered light field displays and is also adaptable to other mobile, head-mounted [32], tabletop [33] or autostereoscopic displays.

We plan to extend the proposed idea to light field displays with more than three light attenuating layers in our future work. Proof-of-concept experiments with our scheme also pave the way to form a more profound understanding in the rank-analysis of a light-field using other mathematically valid

TABLE III: Bjontegaard percentage rate savings for the proposed compression scheme wrt Dib et al. [25]. Negative values represent gains.

Scene	Rank	Circular-2		Hierarchical-2	
		Subset 1	Subset 2	Subset 1	Subset 2
Bikes	4	-97.56541214	-99.29882593	-98.3907291	-99.54258115
	8	-95.76892379	-99.03123267	-97.66246664	-99.29956835
	16	-93.17474979	-98.45339444	-96.63095962	-98.95497164
	28	-90.3477664	-98.11361299	-95.58497187	-98.67266268
	44	-87.34955344	-97.75859383	-94.60404741	-98.07437089
	52	-86.18089698	-97.59830221	-94.16664723	-97.93405439
	60	-85.37903466	-97.4382535	-93.89176465	-97.88383496
Stone pillars outside	4	-98.28738998	-99.5671618	-98.54643236	-99.69494577
	8	-97.48146218	-99.45696678	-97.88804729	-99.65675017
	16	-95.3611157	-98.7933481	-96.93436888	-99.10493755
	28	-93.25557142	-98.75966092	-95.85758052	-98.75257079
	44	-91.33970709	-98.53538189	-94.86352824	-98.5749095
	52	-91.07697181	-98.45815322	-94.57758068	-98.46705075
	60	-90.76161372	-98.35636369	-94.30087553	-98.40819422
Fountain & Vincent 2	4	-96.27656828	-99.26603902	-96.9530291	-99.57099646
	8	-94.48002919	-98.96179277	-96.34841383	-99.08720888
	16	-91.14745649	-99.02010069	-95.17447177	-99.23270338
	28	-87.71507969	-98.92810522	-93.90335982	-98.97503776
	44	-85.20018338	-98.74257926	-92.71888896	-98.94441882
	52	-84.44629524	-98.77812886	-92.50450918	-98.83289017
	60	-83.73495541	-98.74446465	-92.34241435	-98.90331735

tensor-based models [2], [34] and coded mask cameras [35]. We also aim to verify our scheme with physical light field display hardware. Further, we wish to adapt the proposed scheme with display device availability and optimize the bandwidth for a target bitrate. This would enable deploying the concepts of layered displays on different display platforms that deliver 3D contents with the limited hardware resources, thus, best meeting the viewers' preferences for depth impression or visual comfort.

ACKNOWLEDGMENT

The scientific efforts leading to the results reported in this paper were supported in part by the Department of Science and Technology, Government of India under Grant DST/INSPIRE/04/2017/001853.

REFERENCES

- [1] T. Li, Q. Huang, S. Alfaro, A. Supikov, J. Ratcliff, G. Grover, and R. Azuma, "Light-field displays: a view-dependent approach," in *ACM SIGGRAPH 2020 ET*, pp. 1–2, 2020.
- [2] G. Wetzstein, D. R. Lanman, M. W. Hirsch, and R. Raskar, "Tensor displays: compressive light field synthesis using multilayer displays with directional backlighting," 2012.
- [3] M. Sharma, S. Chaudhury, and B. Lall, "A novel hybrid kinect-variety-based high-quality multiview rendering scheme for glass-free 3d displays," *IEEE TCSVT*, vol. 27, no. 10, pp. 2098–2117, 2016.
- [4] D. Liu, P. An, R. Ma, W. Zhan, X. Huang, and A. A. Yahya, "Content-based light field image compression method with gaussian process regression," *IEEE TM*, vol. 22, no. 4, pp. 846–859, 2019.
- [5] R. J. Monteiro, P. J. Nunes, N. M. Rodrigues, and S. M. Faria, "Light field image coding using high-order intrablock prediction," *IEEE JSTSP*, vol. 11, no. 7, pp. 1120–1131, 2017.
- [6] Y. Li, R. Olsson, and M. Sjöström, "Compression of unfocused plenoptic images using a displacement intra prediction," in *2016 IEEE ICMEW*, pp. 1–4, IEEE, 2016.
- [7] E. Dib, M. Le Pendu, X. Jiang, and C. Guillemot, "Local low rank approximation with a parametric disparity model for light field compression," *IEEE TIP*, vol. 29, pp. 9641–9653, 2020.
- [8] X. Jiang, M. Le Pendu, R. A. Farrugia, and C. Guillemot, "Light field compression with homography-based low-rank approximation," *IEEE JSTSP*, vol. 11, no. 7, pp. 1132–1145, 2017.
- [9] S. Zhao and Z. Chen, "Light field image coding via linear approximation prior," in *IEEE ICIP*, pp. 4562–4566, IEEE, 2017.
- [10] W. Ahmad, S. Vagharshakyan, M. Sjöström, A. Gotchev, R. Bregovic, and R. Olsson, "Shearlet transform-based light field compression under low bitrates," *IEEE TIP*, vol. 29, pp. 4269–4280, 2020.
- [11] Y. Chen, P. An, X. Huang, C. Yang, D. Liu, and Q. Wu, "Light field compression using global multiplane representation and two-step prediction," *IEEE SPL*, vol. 27, pp. 1135–1139, 2020.

- [12] X. Hu, J. Shan, Y. Liu, L. Zhang, and S. Shirmohammadi, "An adaptive two-layer light field compression scheme using gnn-based reconstruction," *ACM TOMM*, vol. 16, no. 2s, pp. 1–23, 2020.
- [13] X. Huang, P. An, F. Cao, D. Liu, and Q. Wu, "Light-field compression using a pair of steps and depth estimation," *Optics express*, vol. 27, no. 3, pp. 3557–3573, 2019.
- [14] B. Hériard-Dubreuil, I. Viola, and T. Ebrahimi, "Light field compression using translation-assisted view estimation," in *2019 PCS*, pp. 1–5, IEEE, 2019.
- [15] I. Schiopu and A. Munteanu, "Deep-learning-based macro-pixel synthesis and lossless coding of light field images," *APSIPA TSIP*, vol. 8, 2019.
- [16] D. Liu, X. Huang, W. Zhan, L. Ai, X. Zheng, and S. Cheng, "View synthesis-based light field image compression using a generative adversarial network," *Information Sciences*, vol. 545, pp. 118–131, 2021.
- [17] D. Liu, L. Wang, L. Li, Z. Xiong, F. Wu, and W. Zeng, "Pseudo-sequence-based light field image compression," in *IEEE ICMEW*, pp. 1–4, IEEE, 2016.
- [18] W. Ahmad, R. Olsson, and M. Sjöström, "Interpreting plenoptic images as multi-view sequences for improved compression," in *IEEE ICIP*, pp. 4557–4561, IEEE, 2017.
- [19] W. Ahmad, M. Ghafoor, S. A. Tariq, A. Hassan, M. Sjöström, and R. Olsson, "Computationally efficient light field image compression using a multiview hevc framework," *IEEE access*, vol. 7, pp. 143002–143014, 2019.
- [20] J. Gu, B. Guo, and J. Wen, "High efficiency light field compression via virtual reference and hierarchical mv-hevc," in *IEEE (ICME)*, pp. 344–349, IEEE, 2019.
- [21] K. Maruyama, K. Takahashi, and T. Fujii, "Comparison of layer operations and optimization methods for light field display," *IEEE Access*, vol. 8, pp. 38767–38775, 2020.
- [22] M. Le Pendu, C. Guillemot, and A. Smolic, "A fourier disparity layer representation for light fields," *IEEE TIP*, vol. 28, no. 11, pp. 5740–5753, 2019.
- [23] C. Musco and C. Musco, "Randomized block krylov methods for stronger and faster approximate singular value decomposition," *arXiv preprint arXiv:1504.05477*, 2015.
- [24] G. J. Sullivan, J.-R. Ohm, W.-J. Han, and T. Wiegand, "Overview of the high efficiency video coding (hevc) standard," *IEEE TCSVT*, vol. 22, no. 12, pp. 1649–1668, 2012.
- [25] E. Dib, M. Le Pendu, and C. Guillemot, "Light field compression using fourier disparity layers," in *IEEE ICIP*, pp. 3751–3755, IEEE, 2019.
- [26] S. J. Gortler, R. Grzeszczuk, R. Szeliski, and M. F. Cohen, "The lumigraph," in *Proceedings of the 23rd annual conference on Computer graphics and interactive techniques*, pp. 43–54, 1996.
- [27] M. Levoy and P. Hanrahan, "Light field rendering," in *Proceedings of the 23rd annual conference on Computer graphics and interactive techniques*, pp. 31–42, 1996.
- [28] M. Gu and S. C. Eisenstat, "Efficient algorithms for computing a strong rank-revealing qr factorization," *SIAM Journal on Scientific Computing*, vol. 17, no. 4, pp. 848–869, 1996.
- [29] M. Rerabek and T. Ebrahimi, "New light field image dataset," in *8th International Conference on QoMEX*, 2016.
- [30] D. G. Dansereau, O. Pizarro, and S. B. Williams, "Decoding, calibration and rectification for lenselet-based plenoptic cameras," in *Proceedings of the IEEE conference on computer vision and pattern recognition*, pp. 1027–1034, 2013.
- [31] G. Bjontegaard, "Calculation of average psnr differences between rd-curves," *VCEG-M33*, 2001.
- [32] V. Thumhuri and M. Sharma, "A unified deep learning approach for foveated rendering & novel view synthesis from sparse rgb-d light fields," in *IC3D*, Brussels, Belgium, 2020.
- [33] K. Maruyama, H. Kojima, K. Takahashi, and T. Fujii, "Implementation of table-top light-field display," in *IDW*, 2018.
- [34] Y. Kobayashi, K. Takahashi, and T. Fujii, "From focal stacks to tensor display: A method for light field visualization without multi-view images," in *IEEE ICASSP*, pp. 2007–2011, IEEE, 2017.
- [35] K. Maruyama, Y. Inagaki, K. Takahashi, T. Fujii, and H. Nagahara, "A 3-d display pipeline from coded-aperture camera to tensor light-field display through cnn," in *IEEE ICIP*, pp. 1064–1068, IEEE, 2019.